National Physical Laboratory

NPL REPORT MS 4

Tools for Continuous Modelling Case Study 1: the laser flash experiment

Lindsay Chapman, Clare Matthews, Simon Roberts, Louise Wright, Xin-She Yang

November 2010

National Measurement System

Tools for Continuous Modelling Case Study 1: the laser flash experiment

Lindsay Chapman, Clare Matthews, Simon Roberts, Louise Wright, Xin-She Yang
Mathematics and Scientific Computing Group

November 2010

ABSTRACT

This report describes the application of sensitivity analysis and optimisation methods to a simulation of a laser flash thermal diffusivity experiment. The aim of the work was to calculate estimates of thermal conductivities of materials within layered samples that cannot be measured directly, and to understand how other unknown parameters (laser power, emissivity) affect the calculated values. The sensitivity and optimisation work builds on the results of earlier investigations reported in *Sensitivity analysis, optimisation, and sampling methods applied to continuous models* [10] and *Sensitivity analysis, optimisation, and sampling methods applied to continuous models: three test cases* [11].

NPL Report MS 4

ISSN 1754–2960

National Physical Laboratory,
Hampton Road, Teddington, Middlesex, United Kingdom TW11 0LW

We gratefully acknowledge the financial support of the UK Department for Business, Innovation and Skills (National Measurement Office)

Approved on behalf of NPLML by Jonathan Williams,
Knowledge Leader for the Optical Technology and Scientific Computing team

Contents

1 Introduction

The case study reported here forms part of the Software Support for Metrology (SSfM) project "Tools for Continuous Modelling and Simulation". The aims of this project are to improve the understanding and use of continuous modelling packages and to improve the confidence of model users in the quality of their results. The case studies aim to illustrate the applicability of lessons learnt from the first stages of the project to solving real design problems.

The initial stage of the project compared a number of different sensitivity measures and different sampling and optimisation methods by applying them to three small finite element problems. In addition to highlighting properties of each of the measures and methods tested, this initial work also identified valuable guidelines for developing an efficient methodology to apply to the case studies and to future work in this area. The results of this work are reported in *Sensitivity analysis, optimisation, and sampling methods applied to continuous models* [10] and *Sensitivity analysis, optimisation, and sampling methods applied to continuous models: three test cases* [11].

There are two case studies that apply the methodology developed through the initial small test problems to real-world metrology problems. The case study reported here involves fitting a model to temperature data from a laser flash thermal diffusivity experiment. A description of the experiment is given in section 2. The initial model developed is described in section 3. The definition of the optimisation problem showed some interesting features, and these are described in section 4.

In accordance with the conclusions from the three test problems, a sensitivity analysis was performed on the model prior to the application of any optimisation methods. The results of the sensitivity analysis are described in section 5, and the results of the optimisation process are described in 5.2.

Following the initial analysis, a second model (described in section 6) was developed to address inconsistencies between the model predictions and measurement data. Results from optimisation runs on the second model, described in section 6.2, allow comparison of the two different models of the experiment. Section 6.2 also includes the results of an investigation into the effects of some of the experimentally-determined quantities associated with the measurement data.

This report focuses on the results and conclusions drawn from the sensitivity analysis and optimisation process. The sensitivity indices and optimisation algorithms are not described in this report. Greater details of the methods applied to generate these results can be found in the companion reports [10, 11].

1.1 Thermal properties of materials

The laser flash experiment measures the thermal diffusivity of materials. Thermal diffusivity is a measure of how quickly heat travels through a material and has units of $m^2\ s^{-1}$. Thermal diffusivity α is related to density ρ, thermal conductivity λ, and specific heat capacity c_p by the equation

$$\alpha = \frac{\lambda}{\rho c_p} \tag{1}$$

A typical steady-state thermal model requires the thermal conductivity of the materials in the model to calculate temperature distributions. Transient thermal models require the user to supply values of density, thermal conductivity and specific heat capacity. Density and specific heat capacity of materials can be measured using other experimental methods, and so thermal conductivity can be calculated from thermal diffusivity using equation (1).

One application of thermal models is to predict the performance of components such as turbine blades or engine components that experience high temperatures and corrosive atmospheres. Such conditions can lead to formation of oxide layers and other compounds on the surface of components, and these layers may not have the same properties as the original material. Accurate predictions of component performance require good estimates of the thermal properties of such layers.

The laser flash experiment and its associated data processing method (described in section 2.2) are designed to calculate the thermal diffusivity of isotropic, uniform samples. The aim of the work reported here is to use a numerical model and optimisation techniques to estimate the thermal diffusivity, and hence thermal conductivity, of the individual materials of a layered sample consisting of an oxide layer on the surface of a bulk sample.

1.2 Limitations of this report

This report does not estimate the uncertainties associated with its estimates of thermal conductivity. The main reason for this lack is that the agreement between the experiment and the model is not good enough to consider the model to be fully validated. The lack of uncertainty estimation means that no uncertainties have been associated with the input quantities and no investigations of the experimental repeatability have been undertaken. The work reported here considers a data set gathered during a single measurement of a sample.

If further improvements were made to the model then uncertainties could be estimated using the various sampling methods described elsewhere [10, 11]. It has not been possible to make these improvements during this project.

2 Experiment

This section describes the experimental set-up required to carry out the measurement and the data processing technique used to obtain the thermal diffusivity from the measurements.

2.1 Equipment

The experiment exposes one circular face of a cylindrical sample of material to a laser flash, and measures the temperature of the opposite face. A diagram of the experimental equipment is shown in figure 1.

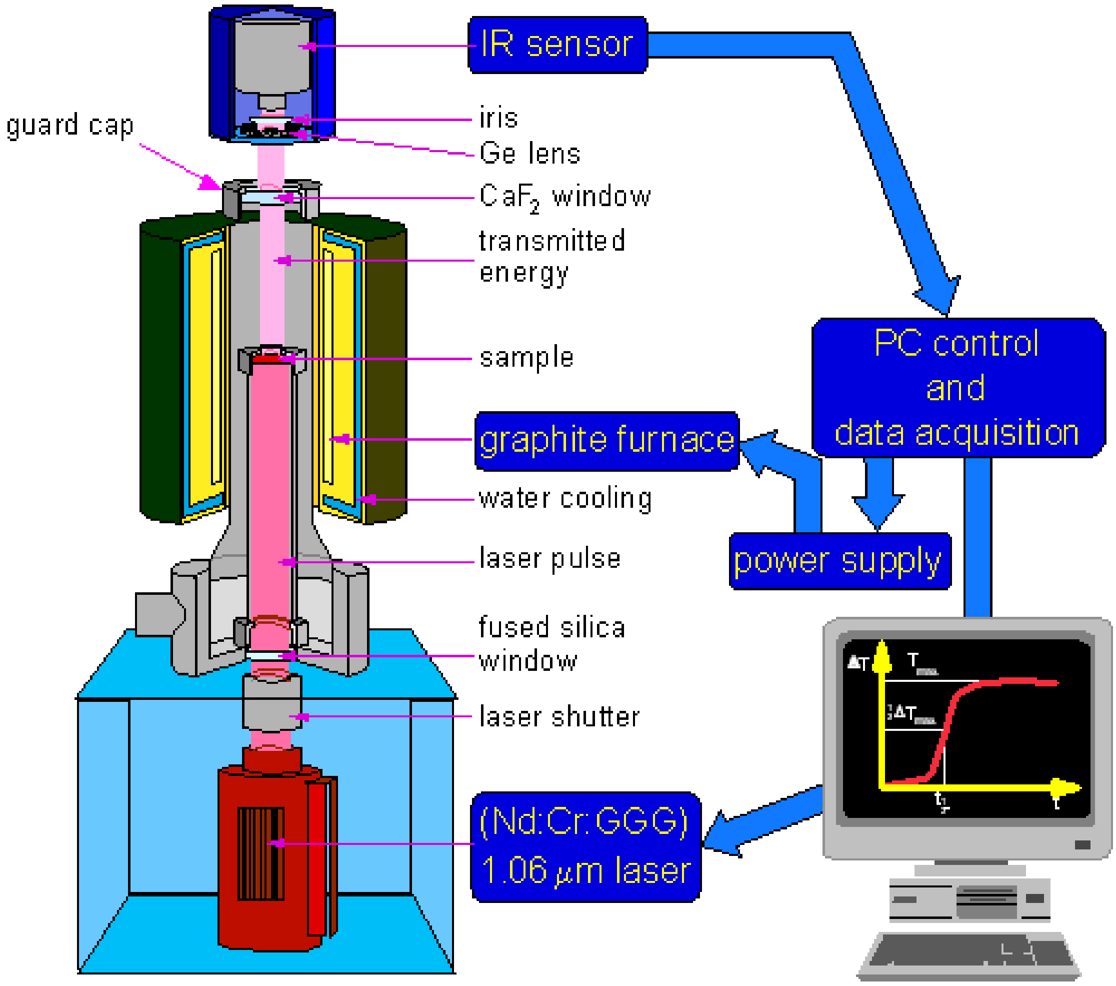

Figure 1: Experimental equipment used in the laser flash thermal diffusivity experiment.

The sample is placed in a furnace so that measurements can be carried out at well-controlled temperatures. The sample is put in the furnace before the experiment starts and the sample is left for a sufficiently long time that there is a vanishingly small probability that the furnace temperature and sample temperature will not be equal. The sample is supported by three small pinsto minimise conductive losses, and the furnace is held in near-vacuum conditions to minimise convective losses. The sample will still lose heat due to radiation.

The laser power is adjusted so that the temperature rise caused by the laser flash is typically between 3 and 4 K. This temperature rise gives a good signal-to-noise ratio on the detected signal, but is sufficiently small that radiative losses can be well approximated by linearisation and can be taken into account in a straightforward manner when calculating the thermal diffusivity. The laser power used is not known by the user and cannot be obtained from the equipment.

The temperature of the rear face of the sample is measured throughout the experiment by an infra-red (IR) temperature sensor. The temperature sensor has a finite spot size and so the measurement is an average over an area rather than at a value taken at a single point.

In order to shield the thermometer from the laser flash, a guard cap with a window in it is placed over the end of the sample (labelled guard cap in figure 1). The guard cap should not be in contact with the material sample since the conductive heat losses from the sample to the cap will affect the measured temperature and hence the calculated thermal diffusivity value. It will be shown in later sections of this report that the data used in this work suggests that there was contact between the guard cap and the sample during the experiment.

2.2 Data processing

The temperature sensor does not measure absolute temperature; instead it supplies a voltage trace that represents the temperature rise with 1 V being equivalent to a rise in temperature of 1 K. The full details of the voltage conversion are not supplied by the instrument manufacturer beyond a statement that 1 V is equivalent to 1 K. The user must know the ambient temperature independently. In this case the ambient temperature is available from the thermocouple controlling the furnace. The voltages are then turned into temperatures by shifting the voltage such that the first measured point is 0 V, and then adding the ambient temperature to each point to obtain the absolute temperature in K.

The data set used in this work consisted of temperature measurements every 1.568 ms. The temperature measurements were continued for 2.373952 s after the laser flash, giving a total of 1515 measurements for $t \geq 0$. It is assumed that the sample temperature has fully stabilised by the time that the laser was fired, and so the temperature measured at $t = 0$ is taken to be the ambient temperature.

A typical set of measurement data is shown in figure 2. The measurement was carried out at an ambient temperature of 947.15 K. This data set was used as target data in the work reported here, meaning that the aim of the optimisation work was to generate model results that fit these data well. This data set was chosen because i) the ambient temperature was sufficiently high that radiative losses would be significant, and ii) the same data set had been studied previously [3], giving values to which the calculated results could be compared.

The time axis is scaled such that the laser was fired at time 0. The small peak shortly after time 0 is caused by energy from the laser flash that has not been absorbed by the sample being measured by the temperature sensor. A close-up of the temperature measurements taken before the laser was fired are shown in figure 3. This close-up of the data suggests that the ambient temperature is drifting very slightly (a straight-line fit to the data shown suggests a drift of 0.17 K s^{-1}), meaning that the ambient temperature when the laser is fired is not necessarily the ambient temperature specified for the experiment. The effects of this offset and drift will be considered in section 6.2.

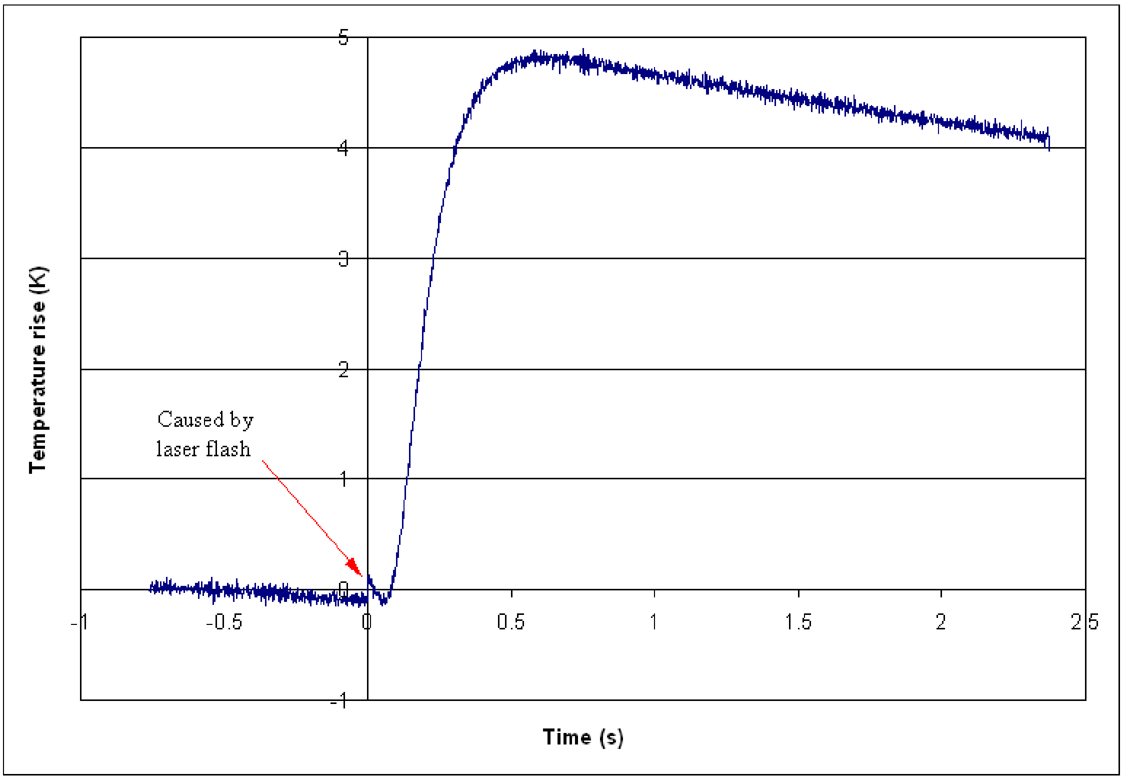

Figure 2: Measured data set used for the work reported here.

The simplest form of data analysis of these data [13] is based on an analytical solution to the transient heat flow equation that assumes a uniform sample, an instantaneous uniform laser flash, and no heat losses from the sample. This approach leads to a 1-D model for the heat flow, and solution of this model gives

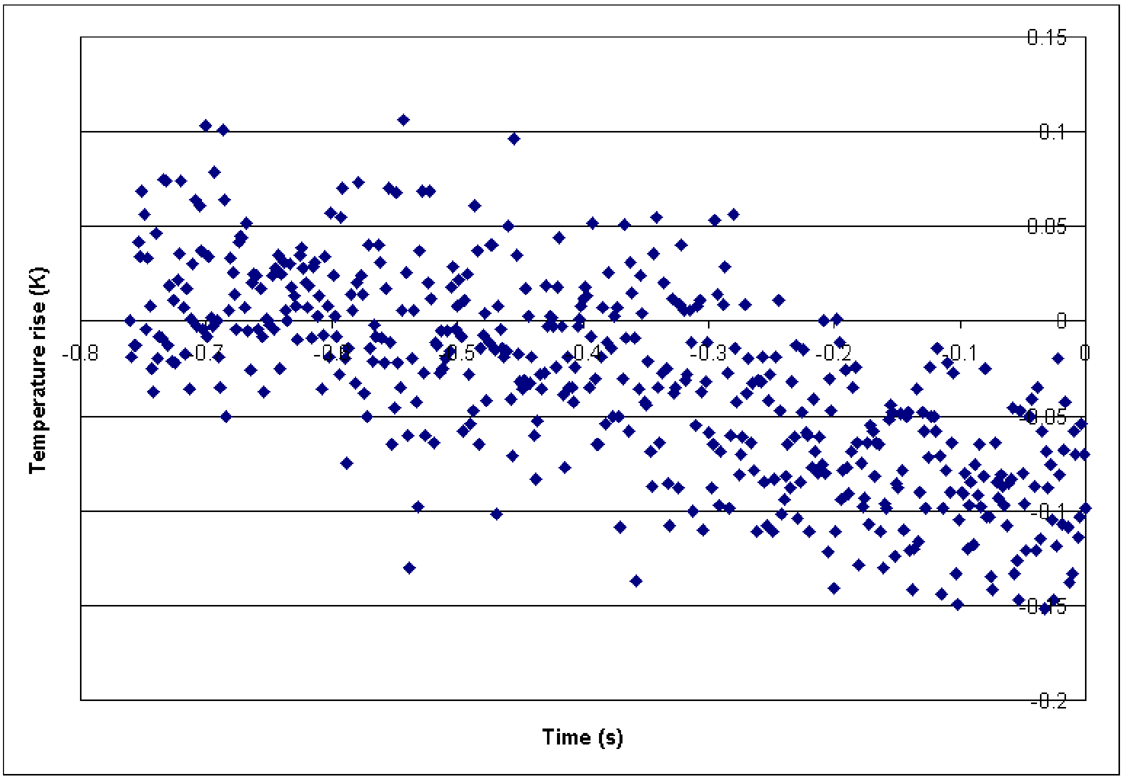

Figure 3: Close-up of the data measured before the laser flash.

an expression of the form

$$\Delta T = T_m \left(1 + 2 \sum_{n=1}^{\infty} (-1)^n \exp(-n^2 \pi^2 \alpha t / L^2) \right) \qquad (2)$$

where $\Delta T(t)$ is the temperature rise of the rear face at time t, ΔT_m is the maximum temperature rise, and L is the thickness of the sample. Defining $t_{1/2}$ as the time taken for the temperature rise to reach half of its maximum value, which can be determined from the measured temperature values, gives

$$\sum_{n=1}^{\infty} (-1)^n \exp(-n^2 \pi^2 \alpha t_{1/2} / L^2) + \frac{1}{4} = 0. \qquad (3)$$

This is a nonlinear equation that gives α in terms of known values. Solving the equation gives

$$\alpha = 0.138785 \frac{L^2}{t_{1/2}} \qquad (4)$$

Subsequent work [4, 7, 9, 16] has developed corrections to the simple 1-D model to allow for the finite duration of the laser pulse and for radiant heat losses (including those from the curved faces). These corrections are implemented within the software that controls the equipment and processes the results. The corrections have not been applied to the data used in the work reported here, because the model described in section 3 includes a finite laser pulse and radiative losses explicitly, and so the model predictions should match the raw data rather than the adjusted data.

The methods of data processing [4, 7, 9, 16] that include corrections still make a number of assumptions, including

- spatial uniformity and isotropy of sample properties,
- temperature variation of material properties during the experiment is insignificant,
- spatial uniformity of the laser flash,
- no conductive or convective heat losses.

The first of these assumptions is clearly not the case for the layered samples of interest in this work. It will be shown in section 3 that the final assumption is not valid for the data used in this work.

2.3 Sample structure and known properties

For the purposes of the modelling work, the sample is assumed to be perfectly cylindrical with plane parallel circular faces of radius 6 mm. The data used in the work reported here were gathered during the measurement of a layered sample. It is assumed in the work reported here that the sample consists of two distinct layers. Each layer is assumed to be uniform and isotropic. The known sizes and properties of the layers in the sample used for the work reported here are listed in table 1. An empty cell indicates that the property is unknown and is to be determined using optimisation methods to minimise the difference between the measured data and the model results. The emissivity, ε, is required for implementation of radiative boundary conditions.

Material	P92 steel	Oxide
Thickness (mm)	2.0942	0.2265
Density (kg m^{-3})	7871	5015
Specific heat capacity (J kg^{-1} K^{-1})	1473.2	934.8
Thermal conductivity (W m^{-1} K^{-1})	45.181	-
Emissivity	0.8	-

Table 1: Thicknesses and thermal properties of the layers. An empty cell indicates that the property is unknown and is to be determined using optimisation.

Previous analysis and simulation of this sample have been described in an NPL report [3]. All properties used in the work reported here have been taken from that report or from the references therein. The full chemical composition of the steel is given in the earlier report. The oxide layer consists of two components, magnetite and iron/chromium spinel, but they have been treated as a single uniform substance in order to provide a simpler model for initial investigations. The model could easily be extended to account for more complex layered structures.

3 Initial model

This section describes the equations and boundary conditions used to define the model of the experiment, and the numerical techniques used to solve the equations.

3.1 Equations, domain, and boundary and initial conditions

The model considers heat flow within the sample and assumes that the heat flow within the rest of the equipment is either irrelevant or can be taken into account via an appropriate choice of boundary conditions. Cylindrical polar coordinates will be used throughout.

The temperature distribution within the sample obeys the transient heat flow equation

$$\rho(\mathbf{x})c_p(\mathbf{x})\frac{\partial T(\mathbf{x},t)}{\partial t} = \nabla.\left(\lambda(\mathbf{x})\nabla T(\mathbf{x},t)\right) + Q(\mathbf{x},t), \tag{5}$$

where $\mathbf{x}$ denotes a position within the sample, $T(\mathbf{x},t)$ is the temperature at a point $\mathbf{x}$ and time t, and $Q(\mathbf{x},t)$ is a heat source term that is used to account for the laser flash.

The domain is defined as $0 \leq r \leq R$, $0 \leq \theta \leq 2\pi$, $0 \leq z \leq L$ where R is the radius of the sample and L is its thickness. It is assumed that the problem is axisymmetric so that variation with θ can be neglected. This reduces the model to two dimensions, making it simpler and quicker to solve.

The domain is split into two layers in the z direction. The properties of each layer are isotropic and uniform and the two layers are assumed to have a perfect thermal bond. The layers are of thickness z_1 (P92) and z_2 (oxide), with $z_1 + z_2 = L$. Then the material properties of the two layers are dependent only on z and are given by

$$\lambda(z) = \begin{cases} \lambda_1 & 0 \leq z \leq z_1 \\ \lambda_2 & z_1 \leq z \leq L \end{cases} \tag{6}$$

$$\rho(z) = \begin{cases} \rho_1 & 0 \leq z \leq z_1 \\ \rho_2 & z_1 \leq z \leq L \end{cases} \tag{7}$$

$$\varepsilon(z) = \begin{cases} \varepsilon_1 & 0 \leq z \leq z_1 \\ \varepsilon_2 & z_1 \leq z \leq L \end{cases} \tag{8}$$

$$c_p(z) = \begin{cases} c_{p1} & 0 \leq z \leq z_1 \\ c_{p2} & z_1 \leq z \leq L \end{cases} \tag{9}$$

The source term Q is assumed to affect a uniform layer (thickness Δz) at the front of the sample directly. It is assumed that the flash is of equal intensity over its finite duration. If the duration is t_0 and the intensity is I then

$$Q(z,t) = \begin{cases} I & 0 \leq z \leq \Delta z,\ 0 \leq t \leq t_0 \\ 0 & \text{otherwise} \end{cases} \tag{10}$$

The value of I is not know a priori and must be estimated during the optimisation process. A value for t_0 is known from the experiment and a value for Δz will be assigned when the numerical solution method is described in section 3.2. The value of t_0 used in this work was 0.8 ms.

The initial conditions are to assume that the sample is uniformly at the ambient temperature T_0 at time 0, so that $T(r, z, 0) = T_0, 0 \leq r \leq R, 0 \leq z \leq L$.

Initially it was assumed that the downward slope of the temperature curve after it reached its peak could be accounted for entirely by radiation. A straight-line fit to the cooling section of the curve shows a cooling rate of approximately 0.42K s^{-1}. A simplified model assuming instantaneous uniform temperature change throughout the sample during cooling shows that the maximum radiative heat loss for a sample of this type at an ambient temperature of 947.15 K and a sample temperature of 952.15 K is approximately 0.02 K s^{-1} (this value is likely to be an overestimate due to the model assumptions). This finding was backed up by runs of a one-dimensional model (see section 3.2 for more details) with only radiative cooling which showed a poor fit to the cooling section of the curve. These findings mean that the cooling of the sample must involve another method of heat loss in addition to radiative cooling.

Considering the experimental set-up, the most likely source of extra heat loss from the sample is contact between the guard cap indicated in figure 1 and the sample. This contact could be caused by thermal expansion of the sample, the sample being too large for the holder, or poor positioning of the sample within the holder.

The cross section of the guard cap is shown in figure 4, including dimensions. The cap has a window at its centre through which the sample temperature is measured and which is transparent to IR. The radiative losses of the sample pass through this window. It is initially assumed that there is a perfect thermal bond between the surface of the guard cap marked with a heavy line (red in colour and online versions) and the equivalent portion of the sample, and that the guard cap is uniformly at the ambient temperature. These assumptions avoid the need to include the heat flow within the guard cap in the model and enable the heat loss to be modelled as a boundary condition.

The curved surfaces are assumed to be perfectly insulated. The temperature gradient along the axis of symmetry must be zero. The flat face exposed to the laser is assumed to lose heat radiatively. These boundary conditions can be expressed as

$$\left.\frac{\partial T}{\partial r}\right|_{r=0} = 0, \quad 0 \leq z \leq L, \tag{11}$$

$$\left.\frac{\partial T}{\partial r}\right|_{r=R} = 0, \quad 0 \leq z \leq L, \tag{12}$$

$$\left.\frac{\partial T}{\partial z}\right|_{z=0} = \varepsilon\sigma(T(r,0,t)^4 - T_0^4), \quad 0 \leq r \leq R \tag{13}$$

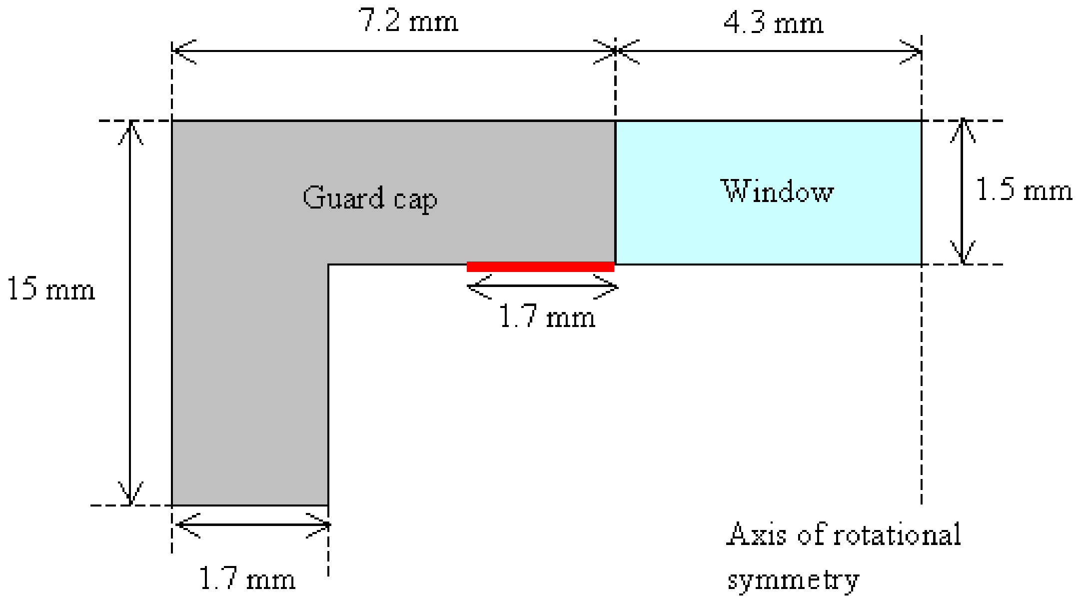

Figure 4: Sketch of the guard cap geometry (not to scale). Red area marks the region of contact between guard cap and sample.

$$\left.\frac{\partial T}{\partial z}\right|_{z=L} = -\varepsilon\sigma(T(r,L,t)^4 - T_0^4), \quad 0 \leq r \leq r_w \tag{14}$$

$$T(r,L,t) = T_0 \quad r_w < r \leq R \tag{15}$$

where r_w is the radius of the window in the guard cap and σ is the Stefan-Boltzmann constant.

These equations, boundary conditions, initial conditions, and material properties fully define the two-dimensional model. The model cannot be solved analytically, in part due to the radiative conditions causing nonlinearity. A numerical approximation technique must be used instead.

3.2 Numerical solution method

The technique used to solve the model numerically is based on the finite volume method. The structure and approach are described in detail elsewhere [3, 8]. The finite volume method calculates the net change in the value of the quantity of interest within a small volume over a short time by calculating the fluxes over each of the faces of the volume during that time. The fluxes are typically gradient terms, which are approximated using finite difference techniques, and are balanced between adjacent cells. The main difficulties are the correct handling of boundaries between different materials and the correct implementation of boundary conditions. The model used here calculates the temperatures at the centre of each volume at a series of time steps.

The work reported here has used a version of TherMol [3, 8], an NPL software package for multiphysics applications focussing on the diffusion equation, as the basis for the model. The software used has been adapted from a three-dimensional SciLab [1] implementation of TherMol. The main adaptations required have been to allow for two separate regions of boundary conditions on the surface in contact with the guard cap, to allow for use of axisymmetric cylindrical polar coordinates, and to alter some of the input and output features.

The finite volume mesh used two different volume sizes in the z direction, Δz, one for each material. The oxide layer had $\Delta z = 0.0453$ mm and the P92 steel had $\Delta z = 0.0419$ mm. The latter value was used as the value of Δz in the definition of $Q(\mathbf{x}, t)$ in (10). A uniform volume size of $\Delta r = 0.1$ mm was used in the r direction.

An explicit time integration method has been used for the transient calculations for simplicity and ease of implementation. The time step was chosen by trial and error for a typical set of parameter values, and was then divided by 10 to ensure that the model would run for more extreme parameter choices. No numerical stability problems have been encountered during the work.

The results of interest of the model were the temperatures of the rear face averaged over the spot size of the temperature sensor. It was assumed that the temperature sensor spot size was the same size as the window of the guard cap. The model results were output at the same time intervals as the measurements to enable direct comparison.

The software TherMOL has been used before with an optimisation routine to determine unknown properties of the laser flash experiment [3]. The work reported has used a one-dimensional model (assumes axisymmetry and uniformity in the radial direction) with radiative cooling only, and a version of the Nelder-Mead optimisation algorithm, COBYLA [14], able to handle constraints on the parameter values. When applied to the data used in the work reported here, the optimisation process gave a thermal conductivity of 2.1 W m^{-1} K^{-1} for the oxide layer, and a laser power intensity of 1.6×10^8 W m^{-2}, but the model results did not fit the cooling part of the temperature curve. The model results and measurement data are shown in figure 5. The work reported here has attempted to address the discrepancy between model results and measurement data and to see how use of an improved model affects the calculated thermal conductivity and laser power intensity.

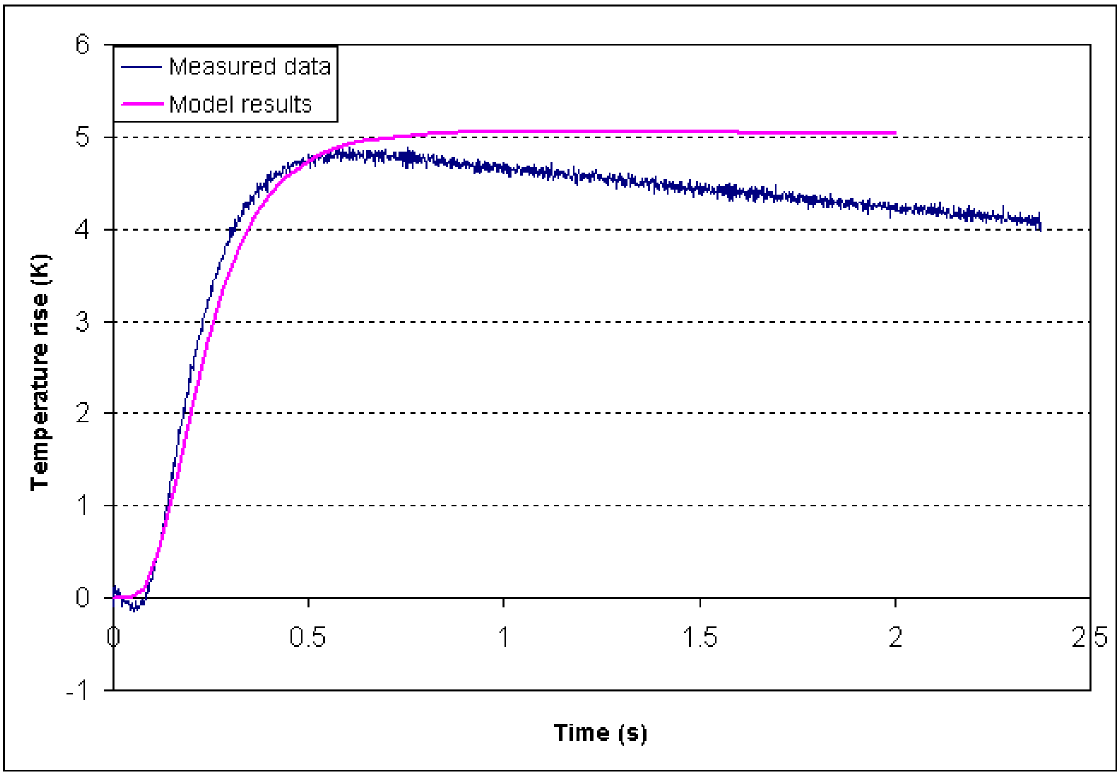

Figure 5: Measured values and model results obtained from earlier work.

4 Definition of the optimisation problem

This section discusses the definition of the optimisation problem. In particular it focusses on the definition of the objective function and how the choice of function affects the optimal parameter values and their associated model results.

4.1 Initial definition of the optimisation problem

The previous sections have mentioned three quantities that are not known from experimental settings or other measurements. These are the thermal conductivity of the oxide layer λ_2, the laser power intensity I, and the emissivity of the oxide layer ε_2. These quantities were used as model parameters in an optimisation process.

The objective function was initially defined as the root mean square average of the relative differences between the measured data and the calculated results:

$$\sqrt{\frac{1}{1515}\sum_{n=1}^{1515}\left(1-\frac{\bar{T}(t_n;\lambda_2,I,\varepsilon_2)}{T_n}\right)^2}, \tag{16}$$

where T_n is the measured temperature at time $t_n = n\Delta t$, and $\bar{T}(t_n;\lambda_2,I,\varepsilon_2)$ is the calculated averaged surface temperature over the spot size of the temperature sensor for a given set of values of the model parameters.

The parameters λ_2 and ε_2 are typically $O(1)$, but I is typically $O(10^8)$ W/m^2. Different parameter scales can cause optimisation algorithms to behave in an unexpected and unpredictable manner. This is because the exploration of the search space by an optimisation algorithm is related to the scales of its unknown parameters. Typically an optimisation algorithm takes steps of a fixed size in various directions as it searches the space. If the parameters are not all of the same order of magnitude, the step size may not be suitable for all the parameters. Rescaling the parameters so that they are all of the same order of magnitude can eliminate this type of problem. Hence the implementation of the model used here was rescaled to expect $O(1)$ input values, and multiplied the relevant input by 10^8 within the model to generate a value of I.

4.2 Initial results

The initial optimisation runs attempted to find the values of λ_2, I, and ε_2 that minimise the objective function (16). The use of this function led to a set of model parameters being identified as optimal values. The optimisation algorithms used (described in more detail in section 5.2) repeatedly converged to $\lambda_2 = 2.41$, $I = 1.50 \times 10^8$, and $\varepsilon_2 = 0.9$. If the model is run with these values of the parameters, the temperature results are as plotted in figure 6. This is clearly a poor fit to the measured data, particularly for $t > 0.25$, but since the optimisation algorithms repeatedly converged to these values it is likely that they are the values that minimise the objective function.

The problem has occured due to the choice of objective function. The lower plot of figure 6 shows a close-up of the first 0.15 seconds. The measured temperatures here are very close to zero, and the model is a very good fit to these values. The small values of T_i for these initial times mean that the relative errors are very large, and so the fit of the model to the data at small times dominates the overall fit. A better choice of objective function in this case would be a root mean square of absolute differences,

$$f = \sqrt{\frac{1}{N}\sum_{i=1}^{N}(\bar{T}_i - T_i)^2}. \tag{17}$$

which would not allow the fit in any part of the data to dominate. In general, if the target data contains values close to zero, absolute differences may be a better choice of objective function than relative differences.

Some trial runs were carried out using the new objective function (17), and the parameter values identified gave a much better overall fit to the measured data. The new objective function has been used throughout the rest of the work reported here, including the sensitivity analysis. The problems experienced illustrate the importance of considering the construction of the objective function carefully. Whilst relative errors can be a good way to combine results of different types, the measured data may not be the best choice of scaling factor.

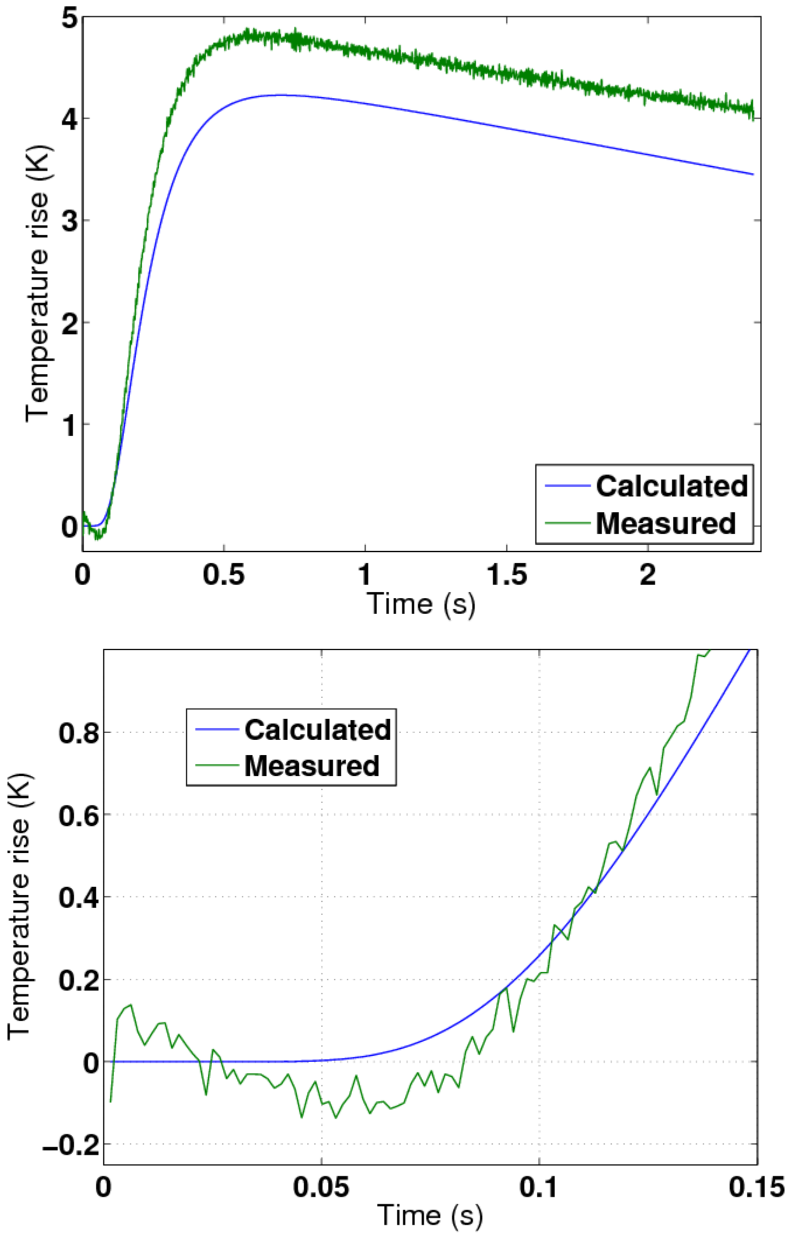

Figure 6: An inappropriate objective function leads to a poor fit of model results to measured data (upper figure), but an unnecessarily good fit to values around 0 (lower figure).

5 Sensitivity analysis and optimisation results

Once the most suitable form of the objective function had been identified, a sensitivity analysis was carried out to identify the most important parameters. This section describes the results of the sensitivity analysis and illustrates how those results can be used to guide the subsequent optimisation runs. The results of the optimisation runs are also reported in this section.

5.1 Sensitivity results

The Morris one-at-a-time (OAT) sensitivity analysis [10, 15] was applied to the laser flash model. Morris OAT analysis calculates elementary effects as the proportional change in the model output for a given change to a single input parameter. The elementary effects capture the strength of dependence of the model results on a given input parameter at a particular value of that parameter. If the elementary effects are calculated at a large number of values of each parameter, conclusions about the global dependence of the results on the parameter can be drawn by comparing the means and standard deviations of the elementary effects associated with each parameter. Approximately 1,500 elementary effects were calculated for each of the three input parameters.

The analysis required limits to be put on the values of the model parameters, and so the following limits were used: 0.1 W m^{-1} K^{-1} $\leq \lambda_2 \leq$ 5 W m^{-1} K^{-1}, 0.5×10^8 W m^{-2} $\leq I \leq 2.5 \times 10^8$ W m^{-2}, $0 \leq \varepsilon_2 \leq 1$. These limits were also used to restrict the search space during the optimisations. The limiting values were obtained by consideration of physical restrictions (values must be positive), estimates of input energy from the laser, and values obtained for λ_2 during earlier work as reported in section 3.2.

The mean, standard deviation and mean absolute value of the elementary effects are given in table 2. The elementary effect statistics imply that of the three input parameters the model is most sensitive to the laser intensity (high mean absolute elementary effect), and least sensitive to emissivity (low mean absolute elementary effect). The difference in the mean value and mean absolute value for each of the parameters suggests that the model output is a non-monotonic function of each parameter. Non-linearity of the objective function may also contribute to the high standard deviation of the laser power elementary effects.

For a model based on only three input parameters, it is straightforward to visualise the model output as a function of these three parameters. A 3D coloured scatter plot, with one axis representing each parameter and the colour of the plotted point representing the model output value, allows consideration of all parameters simultaneously. A 2D coloured scatter plot shows the model output as a function of two input parameters, although the third parameter is also varying with each plotted data point. Data from approximately 6,000 model runs used in the Morris

	λ_2	I	ε_2
Mean EE	-0.087	-0.522	-0.003
S(EE)	0.195	0.697	0.045
Mean |EE|	0.158	0.741	0.038

Table 2: Mean, standard deviation (S) and mean absolute elementary effect (EE) for thermal conductivity (λ_2), intensity (I) and emissivity (ε_2).

OAT analysis were plotted to provide some information on the model response surface. Figure 7 shows the dependence of the objective function on laser intensity and thermal conductivity. Emissivity varies with each data point. Therefore, the smoothness of the objective function in figure 7 is consistent with the lack of sensitivity to emissivity suggested by the Morris OAT analysis.

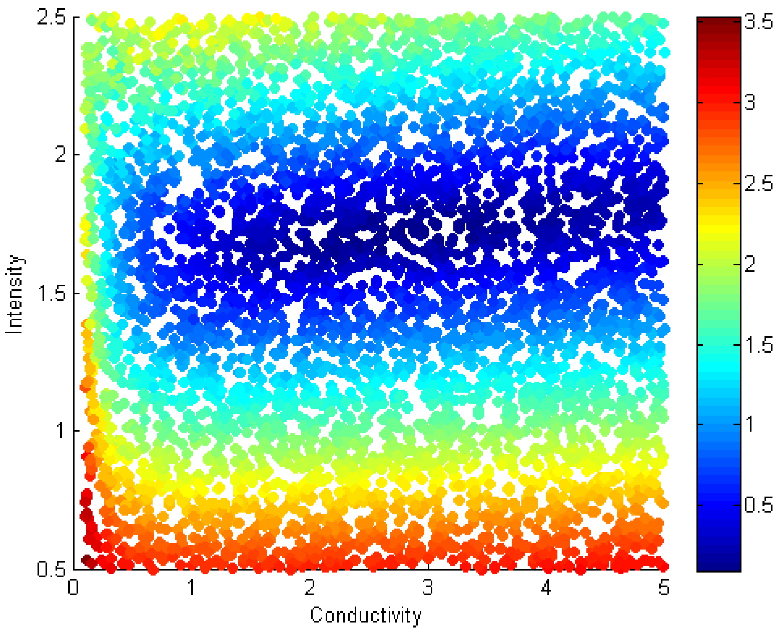

Figure 7: Variation of the objective function with laser intensity and thermal conductivity.

By identifying the most important parameters, and seeing how the objective function varies with these parameters, it is possible to obtain valuable information prior to optimisation. For example, figure 8 provides an estimate of the target value for laser intensity and can be used to apply limits on the parameter values. This can improve the convergence rate of optimisation algorithms. Once a target region has been identified, plotting the data in this area shows whether the objective function varies smoothly and whether the response surface is unimodal (figure 9). These properties will also affect the performance of optimisation algorithms.

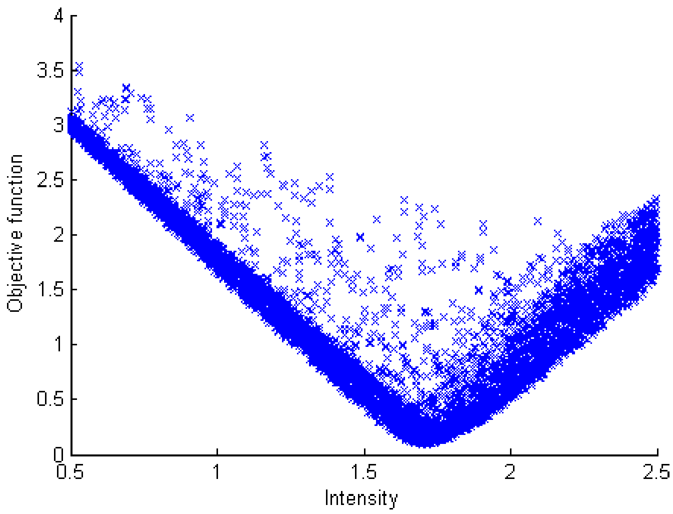

Figure 8: Variation of the objective function with laser intensity.

5.2 Optimisation results

The sensitivity analysis in section 5 suggested that the function is probably smooth and unimodal. A set of extra model runs was carried out to examine the dependency of the function on ε_2 in more detail, and the results are shown in figure 10. The figure shows that the response surface is smooth even in close-up.

The knowledge gained from the sensitivity analysis can be used to guide the choice of optimisation algorithm. Because the surface is smooth and unimodal, an efficient local optimiser such as the Levenburg-Marquardt algorithm within a trust-region [5, 6] should be used. The implementation used in the work reported here is `lsqnonlin` in Matlab's Optimisation Toolbox [2].

A global optimiser has also been used to check that the local optimiser's results are globally optimal. A particle swarm optimisation algorithm (PSO) [12] has been implemented at NPL and this implementation has been used to optimise the same function. By its nature as a global optimiser, PSO can be expected to be slower than trust-region based optimisers such as `lsqnonlin`. At least five sets of optimisation runs have been carried out using each optimisation algorithm and the new objective function. The runs started from randomly-generated points within the parameter search space. The optimal solutions found are summarized in table 3. The results show that both algorithms converged to the same optimal solution.

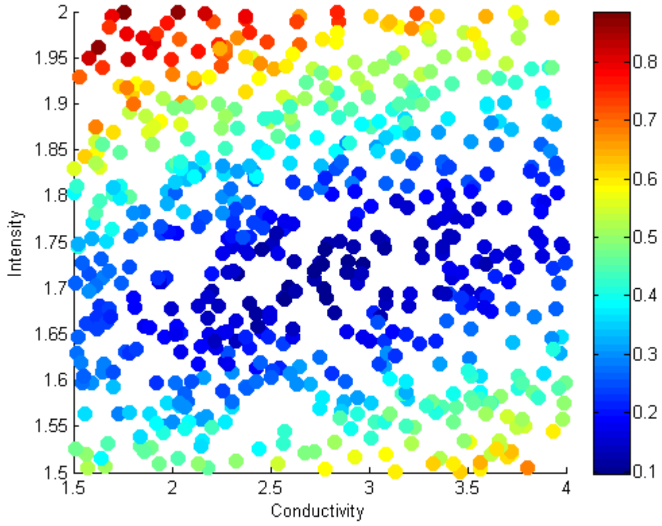

Figure 9: Variation of the objective function with laser intensity and thermal conductivity within the target region of the model.

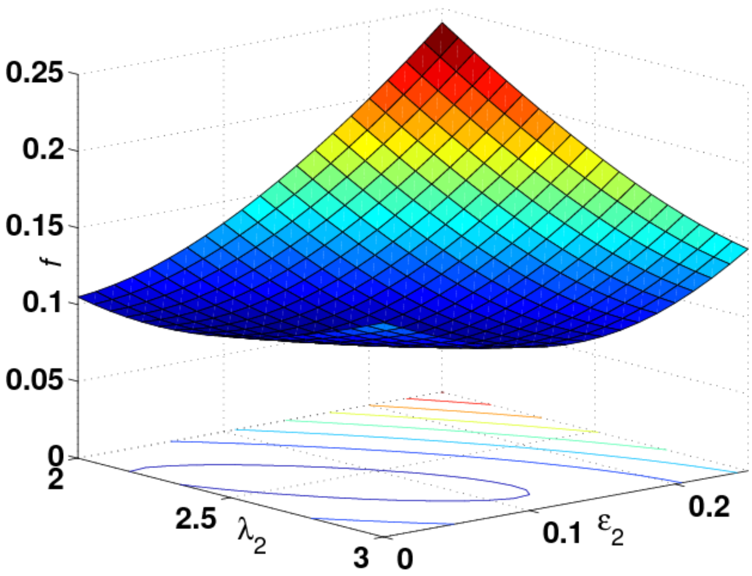

Figure 10: Response surface constructed from a regular grid of λ_2 and ε_2.

	PSO	LSQnonlin
Evaluations	327 ± 56	32 ± 3
Mean/Std	$\lambda_2 = 2.83 \pm 0.23$ $I = 1.69 \pm 0.12$ $\varepsilon_2 = 0.092 \pm 0.073$	2.82 ± 0.005 1.69 ± 0.04 0.0000 ± 0.002

Table 3: Summary of optimisation results. Means and standard deviations of parameters calculated from 5 runs. Note that intervals specified here are ±one standard deviation.

The PSO also showed more variation within the five runs than `lsqnonlin`, leading to a higher standard deviation for each of the parameters. As expected, PSO required more function evaluations (about 327) to converge than the efficient local optimiser (about 32). As stated in section 5, earlier work had found values of $\lambda_2 = 2.1$ W m^{-1} K^{-1} and $I = 1.6 \times 10^8$ w m^{-2}, which is a change of about 25% in the value of λ_2.

The results of the model obtained by using the optimal parameter values are shown in figure 11. These model results are clearly a better fit to the measured data than those shown in figure 6, illustrating the value in changing the objective function. They are also a better fit to the measured values than the results shown in figure 5, illustrating that the new model is an improvement to the previous version.

There is still a discrepancy in the cooling part of the curve where the model results appear to cool too fast. Additionally, the value of ε_2 that has been found is unexpectedly low (physically the value must be between 0 and 1, and was expected to be close to 0.8). These observations suggest that the model needs to be revised in order to simulate the experiment more accurately. It is also possible that the conductive cooling through the contact with the guard cap dominates the cooling part of the curve to such an extent that it may not be possible to determine the emissivity.

6 Revised model

This section describes the revisions made to the model in the light of the initial optimisation results described in section 5.2, and presents the results of the optimisations carried out using the revised model. The revised model was also used to consider the effects of the thermal drift shown in figure 3 and inaccurately measured ambient temperature, and the results of those investigations are described in this section.

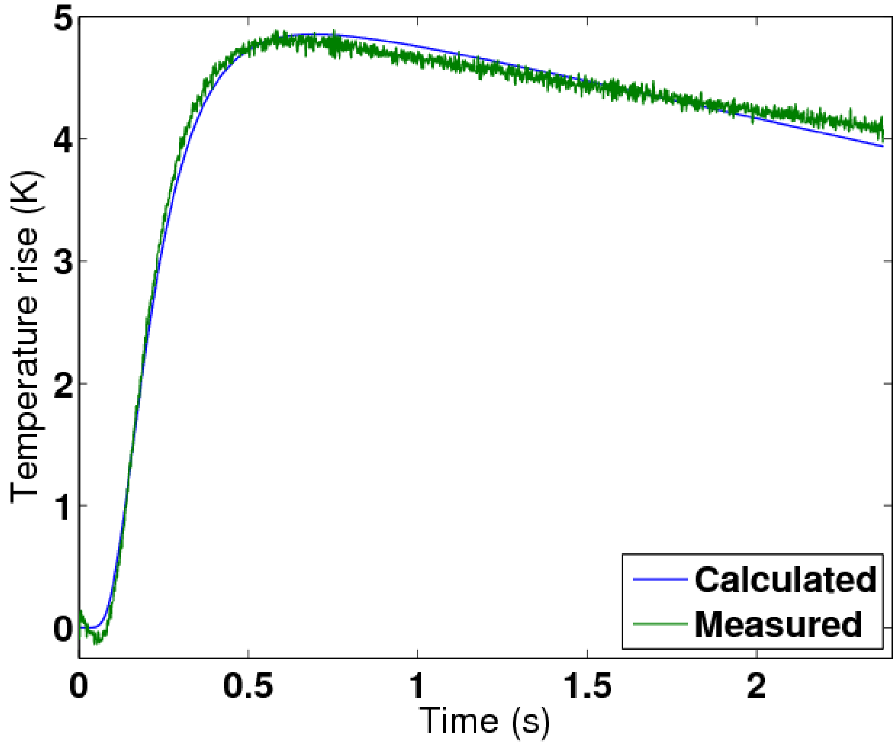

Figure 11: Model results calculated using the best solutions found ($\lambda_2 = 2.8229$, $I = 1.6903 \times 10^8$ and $\varepsilon_2 = 0.0$).

6.1 Model revisions

The results of the initial model suggested that whilst the inclusion of the effects of the guard cap gave a better fit to the measured data, the model was still not predicting the cooling part of the measured data correctly. It was decided that the guard cap should be included in the model as a boundary condition, but the assumption of a perfect thermal bond was removed. The guard cap was still assumed to be uniformly at the ambient temperature.

The use of an imperfect thermal bond introduced a new unknown quantity to the model; the thermal bond quality parameter β with units W m^{-2} K^{-1}. The imperfect bond was defined as an extra layer between the guard cap and the surface of the sample. The bond quality parameter is the thermal conductivity of the extra layer divided by its thickness. The boundary conditions were generated by solving a one-dimensional steady state heat flux equation at each point on the surface in contact with the guard cap, and imposing continuity of temperature and flux at the boundaries of the extra layer. This approach assumes that the only heat flow within the extra layer only occurs in the z direction, which is reasonable because the extra layer is not real and is only a simulation of a poor thermal bond.

These boundary conditions were implemented as

$$\lambda \frac{\partial T(r,z,t)}{\partial z}\bigg|_{z=L} = \frac{\beta\lambda/(\Delta z/2)(T_0 - T(r, L - \Delta z/2, t))}{\beta + \lambda/(\Delta z/2)}, \quad r_w \leq r \leq R. \tag{18}$$

From this implementation it is clear that $\beta = 0$ is a perfectly insulating boundary, and that as $\beta \to \infty$ the condition tends towards a perfect thermal bond with $T(r, L, t) = T_0$ as in the initial model.

An initial investigation was carried out to see how the model results were affected by the value of β and to get practical limits on the values it may take. A full sensitivity analysis was not carried out due to time restrictions. The model was run repeatedly using values of the model parameters λ_2, I and ε_2 that were optimal for the model with a perfect thermal bond, and varying the value of β by an order of magnitude between runs. The results of this exercise are shown in figure 12. The figure shows the temperature vs time curves generated for five values of β. It was found that values of β above 10^6 gave curves that overlaid one another (and overlaid the model with the perfect thermal bond), and that values of β less than 100 gave curves that overlaid one another. The measured data have not been included for clarity.

When the curves shown in figure 12 are compared to the measured data, they suggest that if I and λ_2 do not change significantly then the value of β is likely to be somewhere between 10^4 and 10^7. Since the parameter had a strong effect on the model results β was included in a new set of optimisations and was limited to lie between 0 and 10^7. For the reasons given in section 4.1, the parameter β was rescaled within the model by a factor of 10^6 so that the parameter values used by the optimisation routine were $O(1)$ throughout.

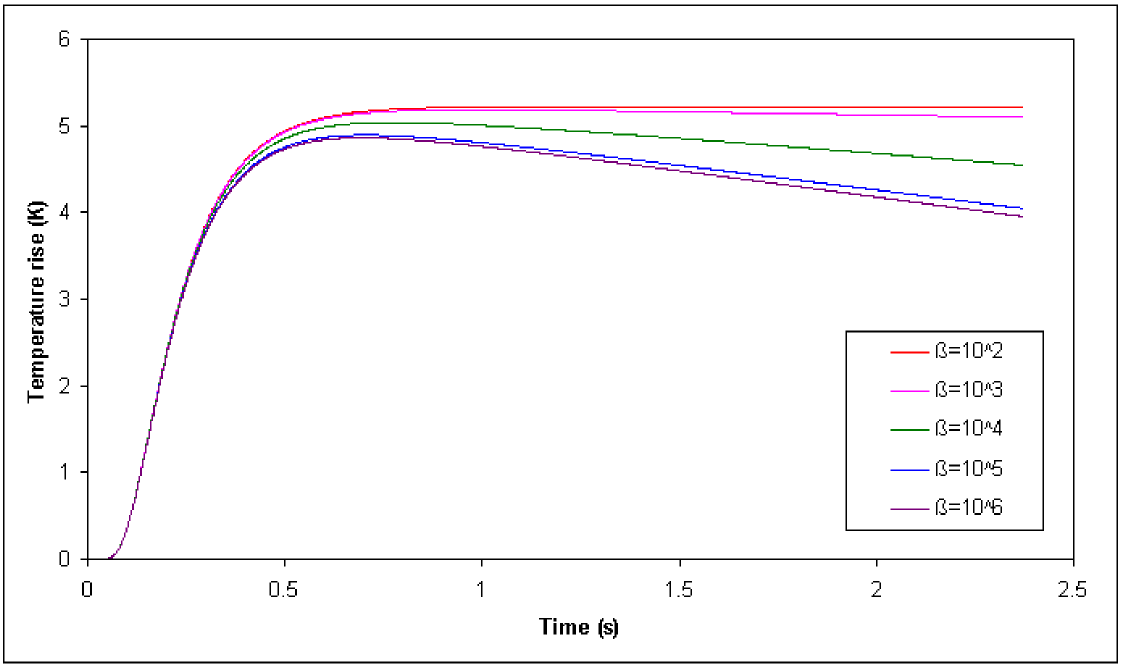

Figure 12: Temperature vs. time model results for various values of the bond quality parameter β.

6.2 Optimisation results with the new model

Following its success on the version of the model with a perfect thermal bond to the guard cap, the optimisations using the new model were carried out using `lsqnonlin`. The new model uses four parameters and so it is expected that more function evaluations will be required to find a converged solution. The optimisation identified the best parameter values as

- λ_2=3.55 W m^{-1}K^{-1},
- I=1.67 $\times 10^8$ W m^{-2},
- ε_2=1.0,
- β=1.92 $\times 10^4$ W m^{-2}K^{-1}.

These values were obtained from five runs, and each run took an average of 126 function evaluations. The standard deviations of each of the parameter values across the five runs were less than 10^{-3}, suggesting good repeatability. The value of λ_2 has increased by about 20 %, and that of ε_2 has gone from 0 to 1, whereas the value of I has not changed significantly. The parameter I defines how much energy goes into the sample during the laser flash, and the good fit of the model

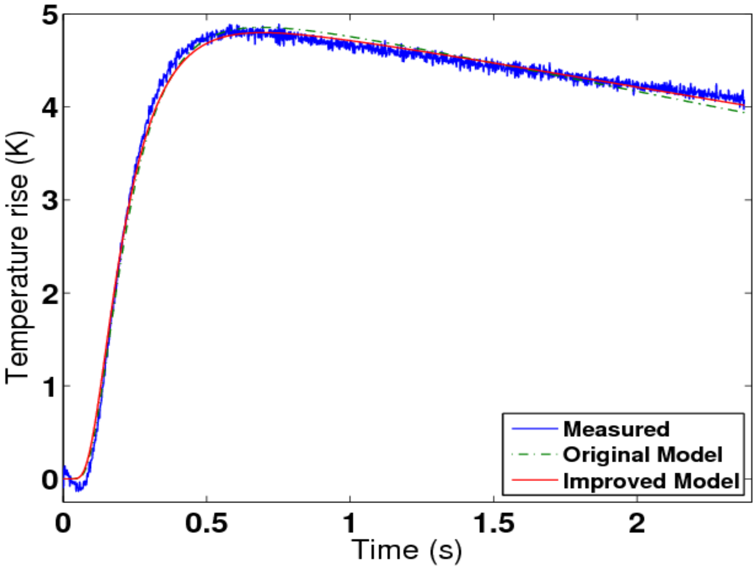

Figure 13: Comparison of new model and original model and their best-fit curves.

results to the peak temperature rise suggests that this value has been determined well. The value of λ_2 affects how the heat flows within the sample, and it seems logical that a change in boundary conditions would affect the optimal value of λ_2. Whilst the new value of ε_2 is closer to the expected value of 0.8, it is by no means certain that this value is a good estimate of the true value. It is likely that the cooling due to the contact with the guard cap still dominates the heat loss, making determination of ε_2 difficult.

The model results obtained by using these parameter values are plotted in figure 13, along with the measured data and the model results shown in figure 11 (dashed line). These plots show that the use of a variable thermal bond quality improves the fit of the model results to the measured data, particularly for $t > 0.5$. The old and new models are in close agreement for $t < 0.3$, which is the time period where the energy absorbed by the sample from the laser flash is likely to dominate the heat flow and differences in the value of λ_2 are less likely to have an effect as the oxide layer is comparatively thin.

It is worth pointing out that the fit, though improved, is still not perfect. Ideally the differences between the model results and measured values would lie below the level of the measurement noise, but this level of agreement has not been achieved. There are differences between the model results and the measured values for $0.3 \leq t \leq 0.5$ which suggest that further improvements could be made to the model. Possibilities for improvements include adding circumferential heat losses, considering an imperfect thermal bond between the sample and the oxide, adding extra layers to allow for the multi-phase nature of the oxide, and including a full model of the guard cap so that the conductive losses are modelled more accurately.

Offset	Optimal Solution ($\lambda_2, I \times 10^{-8}, \varepsilon_2, \beta \times 10^{-6}$)
-0.1	3.2263, 1.6417, 1.0000, 0.0242
-0.01	3.5121, 1.6670, 1.0000, 0.0196
0.0	3.5469, 1.6698, 1.0000, 0.0192
+0.01	3.5823, 1.6726, 0.99999, 0.0188
+0.1	3.9335, 1.6981, 0.9987, 0.0159

Table 4: Optimal parameter values for different offset values. Parameter values are given to a large number of figures so that the trends are clear.

6.3 Effects of thermal drift and ambient temperature

It was shown in figure 3 that the measured temperature drifts slightly between the start of the data logging and the time of the laser flash. The measured temperature at the start of data logging is assumed to be the ambient temperature. As a result, the measured temperature difference from ambient at the time of the laser flash is -0.1 K rather than the expected value of 0 K.

The effects of this temperature drift on the optimal parameters values were investigated in two ways. The first method added an offset to all the data points whilst keeping the ambient temperature used in the model fixed at 947 K. Offsets of ± 0.1 K and ± 0.01 K were used. For each offset a single optimisation run was used to determine the optimal parameter values. The results of these runs are shown in table 4.

The offset required to make the temperature difference at the time of the laser flash 0 K (an offset of +0.1 K) has led to the thermal conductivity value varying by about 10 %, a change consistent with the earlier sensitivity analysis. Whilst this is a small change in absolute terms, it may become more significant for other materials with higher conductivities or for systems with thicker oxide layers. A closer examination of these values suggests that the values of λ_2 and I are approximately linearly dependent on the value of the offset.

An alternative way of looking at the thermal drift is that it represents a change in the ambient temperature. The effects of the ambient temperature not being as stated were tested by repeating the optimisation runs with the original measured temperature differences (no offset) but with different ambient temperatures. The ambient temperature was varied by ± 5 K and ± 2.5 K. The results are shown in table 5. It is clear from this table that the ambient temperature has less effect than an overall offset of the data. The main use of the ambient temperature in the model is in evaluating the radiative heat losses. All other aspects of the model are governed by temperature changes rather than absolute values. Since the maximum temperature rise seen in the model is less than 5 K, radiative losses are quite small and so a variation in ambient temperature makes little difference to the model results.

Ambient T_a (K)	Optimal Solution ($\lambda_2, I \times 10^{-8}, \varepsilon_2, \beta \times 10^{-6}$)
942.15	3.5485, 1.6694, 0.9999, 0.0193
944.65	3.5476, 1.6696, 1.0000, 0.0193
947.15	3.5469, 1.6698, 1.0000, 0.0192
949.65	3.5461, 1.6700, 1.0000, 0.0192
952.15	3.5454, 1.6702, 0.9995, 0.0191

Table 5: Optimal parameter values determined with different ambient temperatures. Parameter values are given to a large number of figures so that the trends are clear.

These results suggest that whilst accurate knowledge of the ambient temperature is not important, the data processing prior to determination of the thermal diffusivity of the sample could be improved by offsetting the data such that the temperature difference is zero when the laser flash is fired. An additional complication that has not been considered here is a constant drift of the temperature: if the ambient temperature continued to drift in the way shown in figure 3 then the best model could involve a varying ambient temperature and it is not clear how this would affect the optimal parameter values.

7 Conclusions

The work reported here has demonstrated the application of sensitivity and optimisation tools to a metrology problem. The work has demonstrated several points of general interest:

- The use of a sensitivity analysis can guide the choice of optimisation algorithm, making the task run more efficiently.
- The choice of objective function in an optimisation can have a very strong effect on the solution, and a small test should be undertaken to check the choice of function is appropriate if possible.

The results of the modelling have also suggested that the contact between the guard cap and the sample may affect the measured values, and hence the calculated thermal diffusivity. The results are also sensitive to the offset of the data, making it important to zero the data at the time the laser pulse is fired rather than when the data logging is started.

The model is still not sufficiently close to the measured data for the uncertainties associated with the model results to be calculable. The most likely methods of model improvement would be a full-scale simulation of the heat flow within the guard cap or a more detailed simulation of the layers within the sample.

References

[1] http://www.scilab.org.

[2] http://www.mathworks.com/products/optimization/.

[3] L. A. Chapman, A. T. Fry, and S. J. Roberts. Thermal diffusivity and thermal conductivity measurements on oxide scales. Technical Report MATC(D)188, NPL, 2004.

[4] L. M. Clark and R. E. Taylor. Radiation loss in the flash method for thermal diffusivity. *J. Appl Phys*, 46:714–719, 1975.

[5] T. F. Coleman and Y. Li. On the convergence of reflective newton methods for large-scale nonlinear minimization subject to bounds. *Mathematical Programming*, 67:189–224, 1994.

[6] T. F. Coleman and Y. Li. An interior trust region approach for nonlinear minimization subject to bounds. *SIAM Journal on Optimization*, 6:418–485, 1996.

[7] R. D. Cowan. Pulse method of measuring thermal diffusivity at high temperatures. *J. Appl Phys*, 34:926–927, 1963.

[8] B. C. Duncan, G. Pilkington, J. S. Nottay, C. R. G. Allen, K. Lawrence, J. Urquhart, and S. J. Roberts. Diffusion of moisture in adhesive bonds. Technical Report DEPC-MPR 062, NPL, 2007. See appendix 1 for details of numerical method.

[9] L. Dusza. Combined solution of the simultaneous heat loss and finite pulse corrections with the laser flash method. *High Temp. High Press.*, 27/28:467–473, 1995/1996.

[10] T. J. Esward, C. E. Matthews, L. Wright, and X.-S. Yang. Sensitivity analysis, optimisation, and sampling methods applied to continuous models. Technical Report NPL Report MS 2, NPL, 2010.

[11] T. J. Esward, C. E. Matthews, L. Wright, and X.-S. Yang. Sensitivity analysis, optimisation, and sampling methods applied to continuous models: three case studies. Technical Report NPL Report MS 3, NPL, 2010.

[12] J. Kennedy and R. C. Eberhart. Particle swarm optimization. In *Proc. of IEEE International Conference on Neural Networks*, pages 1942–1948. IEEE Press, 1995.

[13] W. J. Parker, R. J. Jenkins, C. P. Butler, and G. L. Abbott. Flash method of determining thermal diffusivity, heat capacity and thermal conductivity. *J. Appl. Phys.*, 32:1679–1684, 1961.

[14] M. J. D. Powell. A direct search optimization method that models the objective and constraint functions by linear interpolation. In S. Gomez and J-P. Hennart, editors, *Advances in Optimization and Numerical Analysis.* Kluwer Academic, 1994.

[15] A. Saltelli, K. Chan, and E. M. Scott, editors. *Sensitvity Analysis*, chapter 4. John Wiley and Sons, 2000.

[16] R. E. Taylor and L. M. Clark. Finite pulse time effects in flash diffusivity method. *High Temp.-High Press.*, 6:65–72, 1974.